Inhomogeneous models for plerions: the surface brightness profile of the Crab Nebula

E. Amato[1,2]**, M. Salvati**[3]**, R. Bandiera**[3]**, F. Pacini**[1,3]**, and L. Woltjer**[3,4]

[1] Dipartimento di Astronomia e Scienza dello Spazio, Università di Firenze, Largo E. Fermi 5, 50125 Firenze, Italy
[2] Department of Astronomy, 547 Campbell Hall, University of California, Berkeley, CA 94720, USA
[3] Osservatorio Astrofisico di Arcetri, Largo E. Fermi 5, 50125 Firenze, Italy
[4] Observatoire de Haute-Provence, 04870 Saint Michel l'Observatoire, France

Abstract. We extend the homogeneous model for the synchrotron emission from plerions to allow more realistic predictions of the surface brightness distribution at different frequencies. Abandoning the assumption of a uniform particle distribution, we assume that particles are injected into the synchrotron nebula only in the vicinity of the pulsar. Their distribution is then determined by MHD propagation in a magnetic field of spatially constant but time-dependent intensity. This highly simplified model reproduces the integrated spectrum and the synchrotron surface brightness profile of the Crab Nebula at radio frequencies. However, when applied to higher frequencies, it underestimates the extension of the emitting region, suggesting that particle diffusion with respect to the magnetic field lines must occur.

Key words: ISM: supernova remnants – ISM: individual objects: Crab Nebula – radiation mechanisms: non-thermal

1. Introduction

The integrated non-thermal spectrum of plerionic supernova remnants is well accounted for within the framework of the homogeneous model by Pacini & Salvati (1973, hereafter PS), who regard the plerion as an adiabatically expanding spherical bubble of magnetized relativistic fluid. The bubble is replenished by the continuous conversion of the pulsar's energy outflow into magnetic energy and relativistic particles. The energy balance of the plerion is determined by the competition between the decreasing pulsar's input and the losses the fluid undergoes because of radiation and expansion. Both particles and magnetic field are assumed to be distributed uniformly through the bubble.

When the synchrotron emission of the Crab Nebula is calculated on the basis of the PS model, both the decline of luminosity with time (Véron-Cetty & Woltjer 1991) and the frequency of the low energy spectral break (Marsden et al. 1984) are consistent with a magnetic field strength around 3×10^{-4} G, in agreement with estimates based on equipartition arguments

Send offprint requests to: E. Amato (amato@arcetri.astro.it)

(Woltjer 1958) and also with recent measurements of the nebular inverse Compton radiation flux (De Jager & Harding 1992). Other applications of the PS model include the interpretation of the overall spectral and evolutionary properties of other plerionic supernova remnants, as 3C58 and G11.2-0.3, which seem to be very different from the Crab Nebula (Woltjer et al. 1997).

Despite the success of the model at describing the integrated properties of plerions, the assumption of homogeneity is unsatisfactory. If as assumed the particles are accelerated in the general environment of the pulsar and if loops of magnetic field are created by its rotation, important gradients could be expected in the particle and field distributions. Also observationally such gradients are in evidence. The Crab Nebula does not have a uniform emissivity at any wavelength: it is concentrated towards the center, the more strongly so at the higher frequencies.

We shall here consider a modification of the PS model in which loops of magnetic field are continuously injected with the relativistic electrons attached to the field lines. Since little is known about the detailed conditions around the pulsar we shall assume that the injection takes place at a certain distance r_0 from the center. In the case of the Crab Nebula the moving wisps do in fact suggest that the injection occurs at some $10''$ from the pulsar. Since the propagation velocity of magnetic disturbancies is likely to be much larger than the expansion velocity of the bubble, we shall assume that the field adjusts itself to constant energy density, an assumption that is strictly justified only if the particle pressure is below the magnetic pressure and the field is chaotic.

While in the case of the Crab Nebula the polarization studies at radio and optical wavelengths (Wilson 1972a, Woltjer 1958) indicate a predominance of azimuthal magnetic field, the modest degree of polarization shows that there are different field directions along the line of sight. Such a less regular field (and the effect of reconnection) may well cause the particles to move more freely through parts of the nebula. Thus the present model, which includes only convection, is likely to be a limiting case. In fact we will find that the observed emissivity distribution is intermediate between the one computed here and the homogeneous case.

2. Outline of the model

In our model the nebula is regarded as a sphere of radius $R(t)$, expanding at a constant rate. A continuous supply of new magnetic energy and particles is provided by the central pulsar, whose energy output per unit time can be written as

$$L(t) = \frac{L_0}{(1 + t/\tau)^\kappa}. \tag{1}$$

Both new particles and new magnetic flux are injected into the nebula within a spherical layer at a distance r_0 from the central pulsar. We shall assume that the injection region has zero extension, although very likely this is an oversimplification.

We assume that the particles' velocity distribution is isotropic and that each particle emits essentially at its characteristic frequency: $\nu_c = c_2 B_\perp E^2$, where $c_2 = 0.29 \times (3ec/4\pi(mc^2)^3)$ is a constant, $B_\perp = B\sin\theta$, and E and θ are the particle's energy and pitch angle, respectively. Under these assumptions the nebular synchrotron emissivity becomes

$$S_\nu(\nu, t, r) = \frac{c_1}{2c_2} \int_\Omega \frac{d\Omega}{4\pi} \left(\frac{B_\perp \nu}{c_2} \right)^{\frac{1}{2}}$$
$$\times N\left[\left(\frac{\nu}{c_2 B_\perp} \right)^{\frac{1}{2}}, t, r \right], \tag{2}$$

with $c_1 = (2c/3)(e/mc^2)^4$ a constant and $N(E, t, r)$ representing the particles' spectral and spatial density at time t. The integral represents the average over particles' pitch angles.

As stated before, we regard the magnetic field as spatially constant, therefore, in our model, both the spatial and spectral characteristics of the nebular synchrotron emission are directly related to the particle spatial and spectral distribution, $N(E, t, r)$.

$N(E, t, r)$ is related to the injected particles' spectrum through the particles' number conservation law:

$$N(E, t, r) = \frac{J[E_i(E, t, r), t_i(E, t, r)]}{4\pi r^2} \left| \frac{\partial t_i \partial E_i}{\partial r \partial E} \right|, \tag{3}$$

with J being the number of newly injected particles per unit time and energy interval and E_i and t_i being, respectively, the initial energy and injection time of a given particle. The last term in Eq. (3) represents the jacobian of the transformation $(t_i, E_i) \rightarrow (r, E)$.

Apart from knowledge of the injected spectrum, in order to calculate $N(E, t, r)$ from this equation, knowledge of the particles' age $(t - t_i)$ and initial energy (E_i) as functions of their present position (r) and energy (E) is needed.

We consider the energy evolution of each particle due to adiabatic and synchrotron losses:

$$\frac{dE}{dt} = -\frac{E}{3} \boldsymbol{\nabla} \cdot \boldsymbol{u} - c_1 B^2_\perp E^2. \tag{4}$$

Once the magnetic field $\boldsymbol{B}$ and the fluid bulk velocity $\boldsymbol{u}$ are known at each time, Eq. (4) can be integrated to determine $E_i(E, r)$.

The determination of the time dependence of the magnetic field strength B is straightforward under our assumptions of time constancy of the nebular expansion rate and spatial constancy of B itself. Following PS, we relate B to the nebular content of magnetic energy $W_B(t)$: $B^2(t) = 8\pi W_B(t)/V(t)$, with $V(t) = (4\pi/3)(R^3(t) - r_0{}^3)$ representing the confining volume for the magnetic field. Then we write the time evolution of W_B due to expansion losses and the decreasing pulsar input:

$$\frac{dW_B}{dt} = -\frac{W_B}{3} \frac{d}{dt} \ln V(t) + \beta L(t). \tag{5}$$

Integration of Eq. (5), where β is a constant, yields the magnetic field strength at each time (see, for instance, PS).

Knowing $B(t)$, and further assuming that the magnetic field is largely azimuthal, $\boldsymbol{B} = B(t)\boldsymbol{e}_\phi$, we can use the flux freezing condition,

$$\frac{\partial \boldsymbol{B}}{\partial t} = \boldsymbol{\nabla} \wedge (\boldsymbol{u} \wedge \boldsymbol{B}), \tag{6}$$

as an equation for the fluid bulk velocity $\boldsymbol{u}$, which we assume to be radial: $\boldsymbol{u} = u(r, t)\boldsymbol{e}_r$. Integrating Eq. (6) with the boundary condition that the fluid velocity field matches the expansion velocity of the nebula at its outer edge $(u(R(t), t) = v)$, we find:

$$u(r, t) = \frac{vR(t)}{r} + \frac{\partial \ln B}{\partial t} \frac{(R^2(t) - r^2)}{2r}. \tag{7}$$

The velocity field starts at r_0 at a fraction of the speed of light of order $(v/c) \times (R/r_0)$ ($\sim 1/10$, see below) and then it decreases roughly as $1/r$ to match the nebular expansion velocity at R.

Eq. (7) can also be written as

$$\frac{d}{dt}[B(t)(R^2(t) - r^2(t))] = 0, \tag{8}$$

which yields, in its integral form:

$$B(t)\left(r^2 - r_0{}^2\right) = B(t)\left(R^2(t) - r_0{}^2\right)$$
$$- B(t_i)\left(R^2(t_i) - r_0{}^2\right). \tag{9}$$

This last equation simply states that the magnetic flux injected into the nebula during the time interval $t - t_i$, with t_i being the time at which a particle that at time t is at r was born, is all contained between r_0 and r. Taking $r = r(t, t_i)$ from Eq. (9), we have got the relation needed to connect the particles' position at each time to their age.

Presently what is left to determine, before being able to calculate $N(E, t, r)$ as a function of the injected spectrum, is the evolution of the particles' energy from initial to present value. Introducing the expression found for $\boldsymbol{u}$ into Eq. (4), we obtain:

$$\frac{d}{dt}\left[\frac{1}{E}\left(\frac{B(t)}{r}\right)^{1/3}\right] = c_1 \frac{B(t)^{7/3}}{r^{1/3}} \sin^2\theta. \tag{10}$$

We integrate Eq. (10) after replacing $\sin^2\theta$ with its time average. We take this to be 2/3, which is equivalent to state that each particle during its synchrotron lifetime experiences all the possible velocity orientations with respect to the magnetic field with the same probability. Obviously, we expect this approximation to work better the longer a particle lives, hence the smaller

its initial energy is. Nevertheless we apply it to particles of all energies and finally find the expression for $E_i(E, t, r)$:

$$
\begin{aligned}
E_i(E, t, r) = {} & E \left(\frac{r}{r_0}\right)^{1/3} \left(\frac{B(t_i)}{B(t)}\right)^{1/3} \\
& \times \left(1 - \frac{E}{E_b(t, r)}\right)^{-1}
\end{aligned}
\tag{11}
$$

with

$$
E_b(t, r) = \frac{3}{2c_1} \left(\frac{B(t)}{r}\right)^{1/3} \left(\int_{t_i(r)}^{t} \frac{B(t')^{7/3}}{r(t')^{1/3}} dt'\right)^{-1}.
\tag{12}
$$

The meaning of the energy $E_b(t, r)$ is apparent: it represents the maximum possible energy for particles that at time t reside at r. Substituting E_b with $\sqrt{\nu/(c_2 B_\perp)}$, Eq. (11) also defines the maximum radial distance $r_M(\nu, t)$ from which we expect emission to come for a given frequency.

Inserting our findings into Eq. (3) we are finally able to relate $N(E, t, r)$ to the injected particle spectrum. Concerning the latter some assumptions are necessary. Assuming that the injected electron spectrum is described by a single power law, synchrotron aging can account for just one break in the emission spectrum, while observation shows that in the case of the Crab Nebula there is another break between the optical and the X-rays; this break must be intrinsic to the injection mechanism. Then we allow for a particle energy spectrum with two different slopes in two different energy ranges, namely:

$$
J(E, t) = \begin{cases} K_1(t) E^{-\gamma_1} ; & E_m < E < E_1 \\ K_2(t) E^{-\gamma_2} ; & E_1 < E < E_M \\ 0 ; & E < E_m \text{ or } E > E_M . \end{cases}
\tag{13}
$$

For simplicity, we assume all the energy cuts to be time independent and the ratio between K_1 and K_2 to remain constant. Since we have assumed that a constant fraction β of the pulsar's energy outflow goes into feeding the magnetic field, the remaining $1 - \beta$ will be used for accelerating particles, and then the constraint on the total slowing-down power converted into particles,

$$
(1 - \beta)L(t) = \int_{E_m}^{E_M} J(E, t) E dE,
\tag{14}
$$

implies

$$
K_1(t) \propto K_2(t) \propto L(t).
\tag{15}
$$

Finally we have for the spectral and spatial distribution of particles across the nebula:

$$
\begin{aligned}
N(E, t, r) = {} & \frac{\bar{N}}{(1 + t_i(r)/\tau)^\kappa} E^{-\gamma} \left(\frac{r_0 \, B(t)}{r \, B(t_i(r))}\right)^{\frac{\gamma-1}{3}} \\
& \times \left[1 - \frac{E}{E_b(t, r)}\right]^{\gamma-2} \frac{1}{4\pi r^2} \frac{\partial t_i}{\partial r},
\end{aligned}
\tag{16}
$$

with

$$
\gamma = \begin{cases} \gamma_1, & E_m(r) < E < E_1(r) \\ \gamma_2, & E_1(r) < E < E_M(r) \end{cases}
\tag{17}
$$

where the energies $E_m(r)$, $E_M(r)$ and $E_1(r)$ are the evolved minimum, maximum and intrinsic break energy at radius r, respectively, and can be calculated as functions of E_m, E_M and E_1 by means of Eq. (11).

3. The case of the Crab Nebula

For the Crab Nebula pulsar we have in Eq. (1) $L_0 = 3 \times 10^{39} \text{erg/s}$, $\tau = 710$ yr, $\kappa = (n+1)/(n-1)$ where the braking index n is $n = 2.5$ (Groth 1975). For the parameters of the injected spectrum (Eq. (13)), following a procedure similar to PS, we derive from the observations the values $\gamma_1 = 1.54$, $\gamma_2 = 2.3$, $E_1 \simeq 20 \text{eV}$. The parameter β in Eq. (14) determines, through Eq. (5), the present value of B; we take the latter to be equal to $3 \times 10^{-4} \text{G}$, so that $\beta = 0.25$. Given these parameters the only unknowns in Eq. (16) are the injection radius r_0 and $\bar{N}$, the latter containing the cut-off energies of the injected spectrum. These parameters have very different observational signatures: the first one is related to the radial distance from the central pulsar of the luminosity peak, and the second one only affects the overall nebular synchrotron flux.

The model predictions for the synchrotron surface brightness profile of the Crab Nebula have been compared with high resolution data at various frequencies.

For the radio band we have used a VLA map at a frequency of 1.4 GHz (Bietenholz et al. 1997).

The spatial and spectral distribution of the optical synchrotron continuum was determined by Véron-Cetty & Woltjer (1993) after subtraction of the thermal contributions from foreground stars and filaments, from four narrow-band images at wavelenghts of 9241, 6450, 5364 and 3808 Å. We have reanalysed these maps, kindly put at our disposal by M.P. Véron-Cetty, with state-of-the-art star subtraction algorithms.

Finally, in the X-ray band, we have used, after deconvolution of the instrumental PSF and subtraction of the dust halo (Bandiera et al. 1998), a collection of all the public ROSAT HRI data concerning the Crab Nebula. We have estimated the mean photon energy of these data to be 1 keV.

In our model the synchrotron surface brightness J_ν is simply obtained by integration of Eq. (2) along the line of sight:

$$
J_\nu(\nu, t, z) = \int_z^{R(t)} S_\nu(\nu, t, r) \frac{r dr}{\sqrt{r^2 - z^2}},
\tag{18}
$$

with the expression for the particle number density N in S_ν calculated from Eq. (16).

In order to compare our spherical model with the observations, we have extracted from each image what we call a "radial intensity profile": we first sampled the emission profiles of the nebula along different directions, taking the mean values over small areas of $10'' \times 10''$ and then, after rescaling the different axes to a common length, we averaged those profiles. The procedure just described, to which we refer in the following as "data sphericization", is the main cause of uncertainty in our radial profiles and it is what we take into account in the error bars attached to the data points in the following plots.
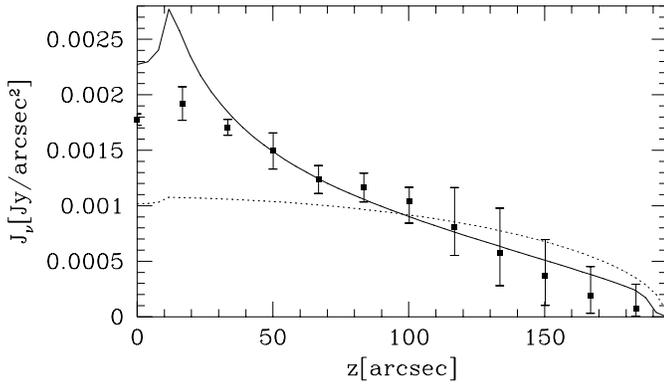
Fig. 1. Comparison with the radio data (points) of the PS model (dotted curve) and of our best fit model (solid curve) for the surface brightness profile of the Crab Nebula. The abscissa is the projected distance from the pulsar. The error bars attached to the data points take into account the uncertainties introduced by "data sphericization".
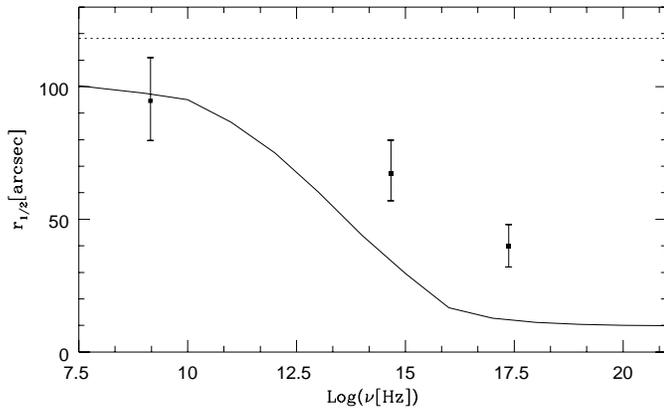
Fig. 2. Comparison with the data at radio (1.4 GHz), optical (6450 Å) and X-ray (1 keV photons) frequencies of the expected size of the emitting region. We plot as a function of frequency the radius within which half of the total nebular flux per unit frequency is produced. The solid curve is based on the present model whereas the dotted curve represents the homogeneous PS model. Again the error bars attached to the data points take into account the effect of our "sphericization" procedure.

When the radiative losses are negligible ($E/E_b(r,t) \ll 1$ in Eq. (16) throughout the entire nebula) $\bar{N}$ and B enter the expression of the synchrotron emissivity simply as multiplying factors. Therefore fitting the shape of the surface brightness profile at radio frequencies allows a straightforward determination of r_0, and once this is known, the value of $\bar{N}$ simply comes from fitting the integrated flux, so that the model is fully determined.

Our best fit estimate gave $r_0 = 10''$, which, for a 2 kpc distance to the Crab Nebula, translates into $r_0 = 0.1$ pc. The corresponding radial profile at 1.4 GHz is plotted against the data in Fig. 1. This value of r_0 yields a distance from the pulsar to the injection site fully compatible with the association between the particle acceleration region and the location of the optical wisps.

As in the PS model, the integrated fluxes reproduce the observations at all frequencies: both the solid and the dashed curve yield the same flux as the interpolation of the data, when integrated on a spherical surface of radius 2 pc. Nevertheless, although in the radio part of the spectrum the fit to the observed profile is rather good and substantially improves the homogeneous model, the model predictions fail to reproduce the data at optical and X-ray wavelengths.

As shown in Fig. 2 the emission at optical and X-ray wavelengths calculated on the basis of the present model is too concentrated: the highest energy particles emit most of their energy immediately after the injection. This causes most of the flux to originate from a narrow region and the particles to travel a very short distance from the injection site before their energy is degraded by severe synchrotron losses.

This effect could be cured by substantially lowering the magnetic field and thereby the synchrotron losses. However the inverse Compton data do not allow this. Moreover if the magnetic field energy is less than the particle energy the model becomes invalid and at lower fields the total particle energy would soon exceed that produced by the pulsar.

The homogeneous PS model in which the particles move freely through the Nebula yields too broad a distribution of the emissivity, our model a too narrow one at the higher frequencies. Apparently some of the particles can reach the outer parts of the nebula without suffering the large synchrotron losses which occur when they are fully tied to the field lines.

Diffusion of particles could solve this problem, but the diffusion coefficient would have to be $\sim 10^4$ times larger than for Bohm diffusion, in agreement with previous estimates (Wilson 1972b). A more complex field structure in which some lines connect the inner and outer parts of the nebula might give an acceptable solution, since the particles could move along these lines at a substantial fraction of the speed of light.

References

Bandiera R., Amato E., Woltjer L., 1998, Mem. Soc. Astron. Ital. 69, 901
Bietenholz M.F., Kassim N., Frail D.A., et al., 1997, ApJ 490, 291
De Jager O.C., Harding A.K., 1992, ApJ 396, 161
Groth E.J., 1975, ApJS 29, 431
Marsden P.L., Gillett F.C., Jennings R.E., et al., 1984, ApJ 278, L29
Pacini F., Salvati M., 1973, ApJ 186, 249 (PS)
Véron-Cetty M.P., Woltjer L., 1991, A&A 251, 31
Véron-Cetty M.P., Woltjer L., 1993, A&A 270, 370
Wilson A.S., 1972a, MNRAS 157, 229
Wilson A.S., 1972b, MNRAS 160, 355
Woltjer L., 1958, Bull. Astron. Inst. Neth. 14, 39
Woltjer L., Salvati M., Pacini F., Bandiera R., 1997, A&A 325, 295